The First Holocene Varve Chronology for the UK: based on the integration of varve counting, radiocarbon dating and tephrostratigraphy from Diss Mere (UK).

Celia Martin-Puertas[1 *], Amy A. Walsh[1], Simon P.E. Blockley[1], Poppy Harding[1], George E. Biddulph[2], Adrian Palmer[1], Arne Ramisch[3], Achim Brauer[3,4]

[1] Department of Geography, Royal Holloway University of London, Egham, Surrey TW20 0EX, UK

[2] School of Geography and Sustainable Development, University of St Andrews, St. Andrews KY16 9AX, UK

[3] Climate Dynamics and Landscape Evolution, GFZ German Centre for Geosciences, 14473 Potsdam, Germany

[4] Institute of Geosciences, University of Potsdam, 14476 Potsdam, Germany

[*] Corresponding author: celia.martinpuertas@rhul.ac.uk

Abstract

The British Isles lack long high-precision and independent chronologies to reconstruct Holocene environmental and climatic conditions at sub-decadal timescales. This paper reports the first Holocene varved chronology for the lacustrine sediment record of Diss Mere in the UK. The record of Diss Mere is 15 m long, and shows 4.2 m of finely-laminated sediments, which are present between ca. 9 and 13 m of core depth. The microfacies analysis identified three major seasonal patterns of deposition (microfacies 1 – 3), which corroborate the annual nature of sedimentation throughout the whole interval. The sediments are diatomaceous organic and carbonate varves with an average thickness of 0.45 mm. Microfacies 1 consists of a pale layer of authigenic calcite crystals and diatom frustules, and a dark layer composed of a planktonic diatoms and filaments of organic matter. Microfacies 2 is similar but includes a mono-specific diatom bloom layer preceding the calcite layer. Microfacies 3 consists of varves with an occasional very thin calcite layer and mono-specific diatom blooms in spring and autumn. A total of 8473 varves were counted with maximum counting error of up to ± 40 varves by the bottom of the varved sequence. To tie the resulting floating varve chronology to the IntCal 2020 radiocarbon timescale, we used a Bayesian Deposition model (*P_Sequence* with outlier detection) on all available chronological data from the core. The data included five radiocarbon dates, two known tephra layers (Glen Garry and OMH-185) with calendar ages based on Bayesian modelling of sequences of radiocarbon ages, and the relative varve counts between dated points. The resulting age-depth model (DISSV-2020) dates the varved sequence between ca. 2100 and 10,300 cal BP and age uncertainties are decadal in scale (95% confidence). The immediate implication of this new UK Holocene chronology is the updated precise ages for the Glen Garry tephra at 2073 ± 39 cal BP and the OMH-185 tephra at 2617 ± 29 cal BP. DISSV-2020 will also enable Holocene research at high time resolution and comparisons to other annually-resolved records on absolute timescales supporting climatic investigations at the regional level.

Keywords: Holocene varve chronology; varve counting; Glen Garry and OMH-185 tephra layers; tephrochronology; Bayesian age modelling

1. Introduction

Holocene palaeoenvironmental and palaeoclimatological studies require precise and accurate chronologies as major changes or transitions between states can occur in less than ten years (Steffensen et al., 2008). Annually-laminated (varved) lake sediments provide an excellent archive to generate varve-based chronologies with age uncertainties usually ranging between 1 to 10% (Ojala et al., 2012). Over short time periods these chronologies can resolve annual-to-decadal scale climatic events that can be detected across, for example, Europe (e.g. Brauer et al., 2008; Martin-Puertas et al., 2012a; Lane et al., 2013; Rach et al., 2014; Martin-Puertas et al., 2019; Palmer et al., 2020). However, varve chronologies for long Holocene records are rare, with sixteen European varved lakes covering the first ~8.5 ka of the Interglacial and only five extending over the last ~10.2 ka (O'Sullivan, 1983; Ojala et al., 2012; Zolitschka et al., 2015; Ramisch et al., 2020). Holocene varve sequences from the British Isles have been reported at only three sites: Loe Pool in Cornwall (Simola et al., 1981); Rostherne Mere in Cheshire (Farr et al., 1991); and Diss Mere in East Anglia (Peglar et al., 1984), although no varve chronology has been published from any of these sites. Consequently, there is significant potential to re-examine varve records from the British Isles to complement those European Holocene varved sequences.

A varve represents one year's sedimentation in former and extant lacustrine and marine environments and is made of, at least, two different sub-layers representing the seasonal pattern of deposition. For any varve study, the development of a process model for the formation of the sub-annual layers is essential. This requires a detailed knowledge of the lake system, its catchment and the climate of the region where the lake is located (Sturm and Lotter, 1995). The seasonal origin of the laminated sediments can be verified by either lake monitoring using sediment traps and / or annual coring of recent sediments at the sediment-water interface, or micro-facies analyses of the laminated sediments identifying seasonal cycle events (e.g. monospecific diatom blooms, layers of authigenic mineral precipitation, detrital deposits associated with spring snow melt, etc). If varves are continuously deposited and preserved from the top of the lake sediment record, varve chronologies provide independent

dating of the sediments; otherwise floating varve chronologies need to be anchored to a calendrical timescale using additional independent dating methods such as radiocarbon and tephrochronology (e.g. Brauer et al., 2000; Wulf et al., 2012).

Tephrochronology requires volcanic ash (tephra) horizons to be identified and then characterised using both their physical properties, and their geochemical and/or mineralogical compositions (Lowe, 2011). The key principle for using tephra as stratigraphic markers and isochrons is that they are erupted and deposited instantaneously (from hours to months), even in marine and lake sediments (Lowe, 2011). Recent improvements in the identification of non-visible, distal tephra layers (cryptotephra) deposited in peat bogs, lakes, marine and aeolian sediments, and ice cores, allow sequences to be linked at distances of hundreds to several thousands of kilometres from the source, greatly extending the tephra's known geographical limit (Blockley et al., 2005, 2007; Davies, 2015). The identification of tephra and cryptotephra deposited in annually-laminated lake records also has advantages by allowing independent varve-dating of tephra layers with errors lower than the original age estimates, and the direct correlation between annually-resolved records (Zolitschka et al., 2000; Lane et al., 2015). Further reductions in age uncertainties can be achieved when radiocarbon, tephrochronology and varve chronologies are integrated within a Bayesian age modelling framework. This approach has been successfully used to anchor varve chronologies in the Late Glacial at European sites, and generating reliable calendar-age models for lake archives that utilise the additional precision provided by the annual timescale (Bronk Ramsey, 2008; Blockley et al., 2008; Palmer et al., 2020).

Currently the Diss Mere sequence reported by Peglar et al. (1984) is assigned to the Holocene through correlation of the Diss Mere pollen stratigraphy to the radiocarbon-dated pollen stratigraphy of central East Anglia (Peglar et al., 1989). The varve sediments at Diss Mere are reported to form from ~2.5 to 5 ka BP (where BP denotes "before AD 1950") through the comparison of the Holocene pollen stratigraphy that cover that varved interval. Consequently, the Diss Mere varved sediments have not been directly dated and it is also unclear what the age interval is for the entire sequence despite the rich palaeoclimate and palaeoecological

113 value of the Diss sediment record (Peglar et al., 1984, 1989; Peglar, 1993a, 1993b; Bailey,
114 2005). Our main goal in this paper is to generate the most precise and accurate chronology
115 possible, which provides the basis for developing the Diss Mere proxy archive at decadal to
116 annual scales. This study presents new data from a coring campaign in 2016 and reports the
117 first varve chronology from the British Isles, which covers most of the Holocene period. This
118 focusses on chronological information from varve counts, radiocarbon dates and cryptotephra
119 horizons along the 5 m long section of continuously, annually-laminated sediments from Diss
120 Mere.
121
122 **2. Regional settings**
123 Diss Mere (52º 22'N, 1º 6'E, 29 m a.s.l.) is a small oval lake (area of 3.4 ha) located in the
124 town of Diss, central East Anglia (England) (Fig. 1a, b). The mere is a eutrophic lake, has a
125 small catchment area (1.5 km^2), without surface inflows and outflows, and a maximum water
126 depth of 6 m. The lake is situated in the River Waveney valley, which was formed during the
127 melting of the Anglian Ice sheet (MIS 12), and the basin is superimposed in places upon the
128 pre-glacial Bytham River valley (Rose, 1994), that is itself cut into the Chalk bedrock and
129 extends, in the region of Diss down to ca 5 m a.s.l.(Lee et al., 2020). The area is mapped as
130 chalky till (Bennett, 1983), which forms a slope to the north and the remainder of the
131 hydrological catchment is encircled by river floodplain and terrace deposits (Wilcox and
132 Stanczszyn, 1983) associated with the River Waveney (Bailey, 2005). Drainage is poor
133 resulting in calcareous groundwater gley soils. The origin of the Mere is unclear, but a possible
134 explanation is related to thermokarst processes during the Younger Dryas (West, 1991). The
135 high water-level in East Anglia during the Late Devensian (West, 1991) combined with a cold
136 climate could have triggered the solution of the Chalk bedrock and led to the formation of the
137 depression. This hypothesis is supported by a 25 m deep borehole at the edge of the mere
138 that shows Lateglacial sediments in the basal 5 m of the sediment sequence. However, the

full thickness of basin infill is unknown, and it is possible that Diss Mere may have formed any time since the Anglian cold stage (Bailey, 2005).

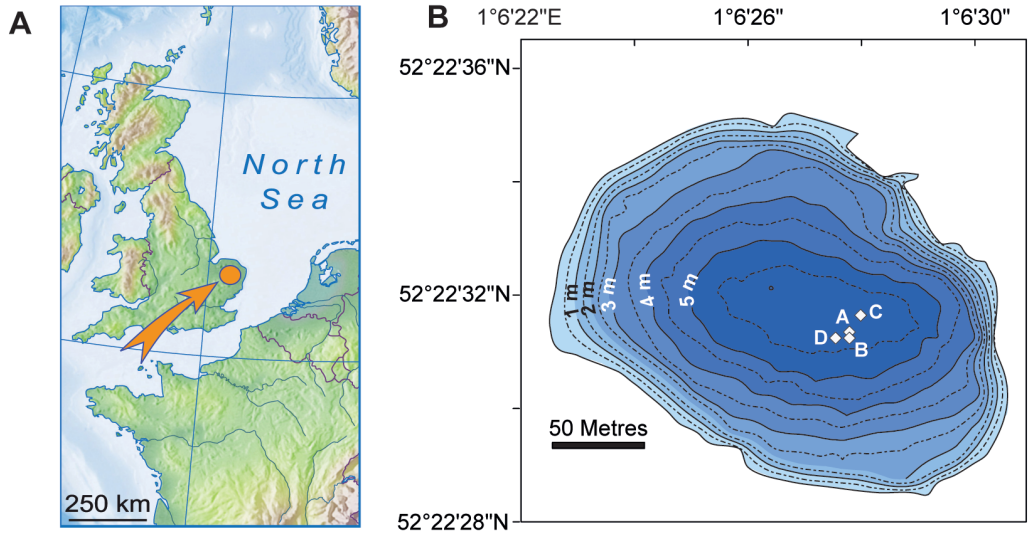

Figure 1. Physical setting of Diss Mere. (**A**) Geographical location of Diss Mere. (**B**) Bathymetry of the lake and coring sites: DISS16-A, 52º 22.523' N, 1º 06.463' E, 5.9 m water depth; DISS16-B, 52º 22.521' N, 1º 06.463' E, 5.9 m water depth; DISS16-C, 52º 22.527' N, 1º 06.466' E, 5.8 m water depth; DISS16-D, 52º 22.521' N, 1º 06.460' E, 5.7 m water depth

3. Previous models of varve formation at Diss Mere

Peglar et al. (1984) identified finely laminated sediments deposited between 9 and 12 m of sediment depth, which were interpreted as varves. These varves are composed of two sub-layers, a pale layer made of calcium carbonate and a dark lamina rich in organic material and sand-sized silica grains. Diatom and chrysophyceae cyst compositions as well as the pollen assemblage was described in detail for fourteen individual pale and dark laminae at 10.85 m of sediment depth. Sediments are rich in diatoms with *Lindavia comta* (Kützing) (Nakov et al., 2015) (previously *Cyclotella comta)* varying between 63-99% of the total diatom assemblage in both the pale and the dark layers. This suggests either *L. comta* having blooms in discrete periods associated with the formation of the pale and dark layers, or a single bloom of sufficient duration that is present in both layers (Peglar et al., 1984). Chrysophyceae cysts are, however, more abundant in the dark layers than in the pale layers suggesting that the formation of the dark laminae starts in late summer and autumn, when the cysts are commonly produced (Tippett, 1964). The pollen composition of the pale (*Tilia and* gramineae) and dark (*Corylus,*

156 *Alnus, Ulmus and Taxus*) layers show a clear pattern of the phenological season
157 distinguishing between plants flowering from May to July and in early spring, respectively. The
158 combination of pollen and chrysophyceae cyst information reveal that the pale (calcite) layer
159 represents lake deposition in late spring and summer (May – July), while the dark (organic)
160 layer indicates accumulation from late summer to late spring (August – April) (Peglar et al.,
161 1984).
162
163 **4. Methods**
164 4.1. Coring and sampling
165 Four parallel sediment cores were obtained in September 2016 from the deepest part of Diss
166 Mere (Fig. 1b, Fig. 2a), using a 90 mm diameter UWITEC piston corer (DISS16-A, B, C and
167 D). Additionally, two gravity cores of 1 m length (DISS16-1S and 2S) were collected from the
168 same area in order to record the present sediments at the sediment-water interface. The
169 maximum distance between cores is 5 m. Core DISS16-A (15.2 m of length) is composed of
170 eight continuous core sections of ca 2 m length and core DISS16-B (13.28 m of length) is
171 made of seven continuous core sections of ca 2 m. Core A was recovered from the
172 water/sediment interface whereas core B starts 100 cm below core A to create an overlap.
173 Cores DISS16-C (7.72 m of length, 4 cores sections of 2 m long) and DISS16-D (5.81 m of
174 length, 3 core sections of 2 m long) start at 6 m and 7 m of sediment depth, respectively.
175 These cores provide two additional parallel sequences of the varved sediment (Fig. 2a). One
176 half of the cores was sub-sampled for sedimentology, cryptotephra investigation and terrestrial
177 macrofossils sampling for radiocarbon dating. The cores were correlated using a total of 67
178 macroscopically visible marker layers and the best-preserved sections were combined to
179 construct the continuous composite profile DISS-16 of 14.5 m length (Fig. 2b).
180 4.2. Varve counting
181 Samples for thin sections were taken from the four piston cores along the finely-laminated
182 sequence (8.88 – 13.15 m of sediment depth). Fresh sediment blocks (10 × 2 × 1 cm) were

183 extracted from the open, split core surface with 2 cm overlaps to enable continuous
184 microfacies analysis, including correlation of marker layers. Thin sections were prepared
185 according to a standard procedure including freeze-drying and impregnation with epoxy resin
186 (Brauer and Casanova, 2001). Detailed microfacies analysis, varve counting, and varve
187 thickness measurements were performed on the petrographic thin sections using a Leica
188 (M205C) stereo-zoom petrological microscope with plane- and cross-polarised light, at 80x.
189 A total of 129 microscopic marker layers were identified in thin sections along the ca 4.2 m
190 long sequence of finely laminated sediments, which were used as tie-points for thin section
191 correlation on a varve-to-varve basis. Varve counting was developed following different steps.
192 First, an overview count of varve numbers between marker layers on the four sediment cores
193 by one counter was carried out. This allowed detection of local disturbances and assigning a
194 varve quality index (VQI) ranging from 4 to 0 (4 = outstanding varve preservation, 3 = good
195 preservation, 2 = preserved varves with changing thickness along the thin section, 1= poor
196 varve preservation, 0 = not laminated sediments). This helped to identify the best-preserved
197 sequences for varve counts and improve the composite profile DISS-16. More precise
198 counting based on thickness measurements for each seasonal layer along the 57 thin sections
199 of the varved composite profile was undertaken by three different counters. A total of four
200 replicate varve-count records were selected to calculate varve count uncertainties (standard
201 deviation and maximum and minimum deviation from the master count record).
202 4.3. Tephra investigation
203 Preliminary investigations through the varved section of the record used contiguous 10 cm
204 'rangefinder' scan samples to ascertain the presence of tephra. Where tephra was identified,
205 higher resolution (1 - 0.5 cm) contiguous samples were analysed to refine the stratigraphic
206 shard profile. All samples were combusted at 550 °C to remove organic matter. Residue
207 material was treated with 10% hydrochloric acid to dissolve calcium carbonate and sieved
208 through 125 and 15 μm mesh. The resulting 125-15 μm fraction was processed for tephra
209 analyses following the method outlined in Blockley et al. (2005) with some minor modifications.
210 To suit the carbonate-rich nature of the sediments, the material was treated with two cleaning

floats of sodium polytungstate (4 ml, density of 2.2 g cm^{-3}) and two extraction floats (4 ml, density of 2.55 g cm^{-3}). The extraction float material was mounted in Canada balsam before optical examination at both 100 x - and 400 x to quantify concentrations as the number of shards per gram of sediment dry weight (Blockley et al., 2005; Timms et al., 2017). Glass-shard major element geochemical analyses were conducted on carbon-coated stubs at the WDS-EPMA (Cameca SX-100) microprobe facility in Edinburgh. The operating conditions for this system used a 3 µm beam size and at 15 keV voltage the following beam currents were employed: 0.5 nA for Al, Na; 2 nA for Mg, Si, K, Ca, Fe and 60 nA for P and Ti (Hayward, 2012). Appropriate internal standards (Lipari and BCR-2G) were analysed to ensure calibration of the microprobe and assess for accuracy and drift.

4.4 Radiocarbon dating and Bayesian age modelling

Radiocarbon dating of the Diss Mere sediments have not been done previously (Peglar et al., 1989; Bailey, 2005). The calcareous nature of the Diss Mere sediments makes the dating of bulk samples unsuitable for radiocarbon dating and good-quality terrestrial macrofossils are scarce. Nonetheless, a total of six samples of terrestrial plant macrofossils from the laminated sequences of the new cores DISS16-A, DISS16-B, DISS16-C and DISS16-D were found and analysed by AMS for ^{14}C dating at Scottish Universities Environmental Research Centre (SUERC) (Table 1). The radiocarbon dates were calibrated with OxCal v4.4.2 (Bronk Ramsey, 2017) using the IntCal20 atmospheric curve (Reimer et al., 2020). Where calendar – year tephra ages of the correlative tephra layers have not been updated since 2020, the original radiocarbon dates have been recalibrated and an age model has been developed using a *P Sequence* deposition model in Oxcal v4.4.2 with a variable K factor (Bronk Ramsey, 2009, 2008; Ramsey and Lee, 2013) (Supplementary information).

Two different deposition models were developed following the approaches outlined in Bronk Ramsey (2008) and Blockley et al. (2008). Both used the selected radiocarbon dates (Table 1) and calendar tephra ages, and the relative varve age between these fixed points as z values within the model, but with slightly different assumptions about the rigidity with which to constrain the varve years between fixed points. The most constrained model used a

239 *U_Sequence* deposition model that assumed there was a uniform rate of deposition of varves
240 between fixed points. The second model that we applied was a *P_Sequence* age model with
241 a fixed K value (0.5 in this case), which allows slightly more variability in the rate of varve
242 deposition but is more rigid than would be the case if a variable K factor was applied. In both
243 models Bayesian outlier detection was applied using the 'general model' at 95% confidence.
244 The 0.5 K value was selected to allow maximum rigidity while not down-weighting any
245 proportion of the dates as outliers.
246
247 **5. Results**
248 5.1. Sedimentology and microfacies analyses
249 New high-quality sediment cores cover the first 15 m of the sediment record of Diss Mere. The
250 basal 2 m are composed of calcareous silt and sand with carbonate concretions, shell
251 fragments and pebble-sized clasts derived from the surrounding diamicton. This unit proved
252 to be impenetrable with this coring system and therefore this was the maximum depth
253 achieved. Three major sediment units are identified in the core material and are broadly
254 comparable to that reported by Peglar et al. (1989). These units are: Unit 1 (0 – 8.90 m)
255 composed of organic-rich mud (lake-gyttja) with intermittent parallel micrite carbonate laminae
256 horizons prevalent at irregular intervals (1 – 2.45 m; 3.72 – 5.48 m; 6.32 – 7 m); Unit 2 (8.90
257 – 13.15 m) is made of finely-laminated sediments with some cm-scale dark greenish massive
258 deposits intercalated. Unit 3 (13.15 – 15 m) is the basal 2 m described above (Fig. 2). The
259 length of the continuous finely laminated sequences (4.27 m) is longer in the composite profile
260 DISS-16 than previously reported by Peglar et al. (1989) and Bailey (2005). It should be noted
261 that Bailey (2005) reports two varved sequences, lithozone B (13.78 – 14.82 m) and lithozone
262 E (9.09 – 11.78 m), which are included in Unit 2 of the DISS-16 stratigraphy through the
263 comparison of core photos. The visual clarity or varve quality and the thickness of the massive
264 deposits is variable between cores (Fig. 2c) that might explain the lack of varve identification
265 by Bailey (2005) between 11.78 and 13.78 m. For example, Bailey (2005) identifies a
266 lithozone C as a 1.27 m-thick peat deposit; we found the same peat deposit in core

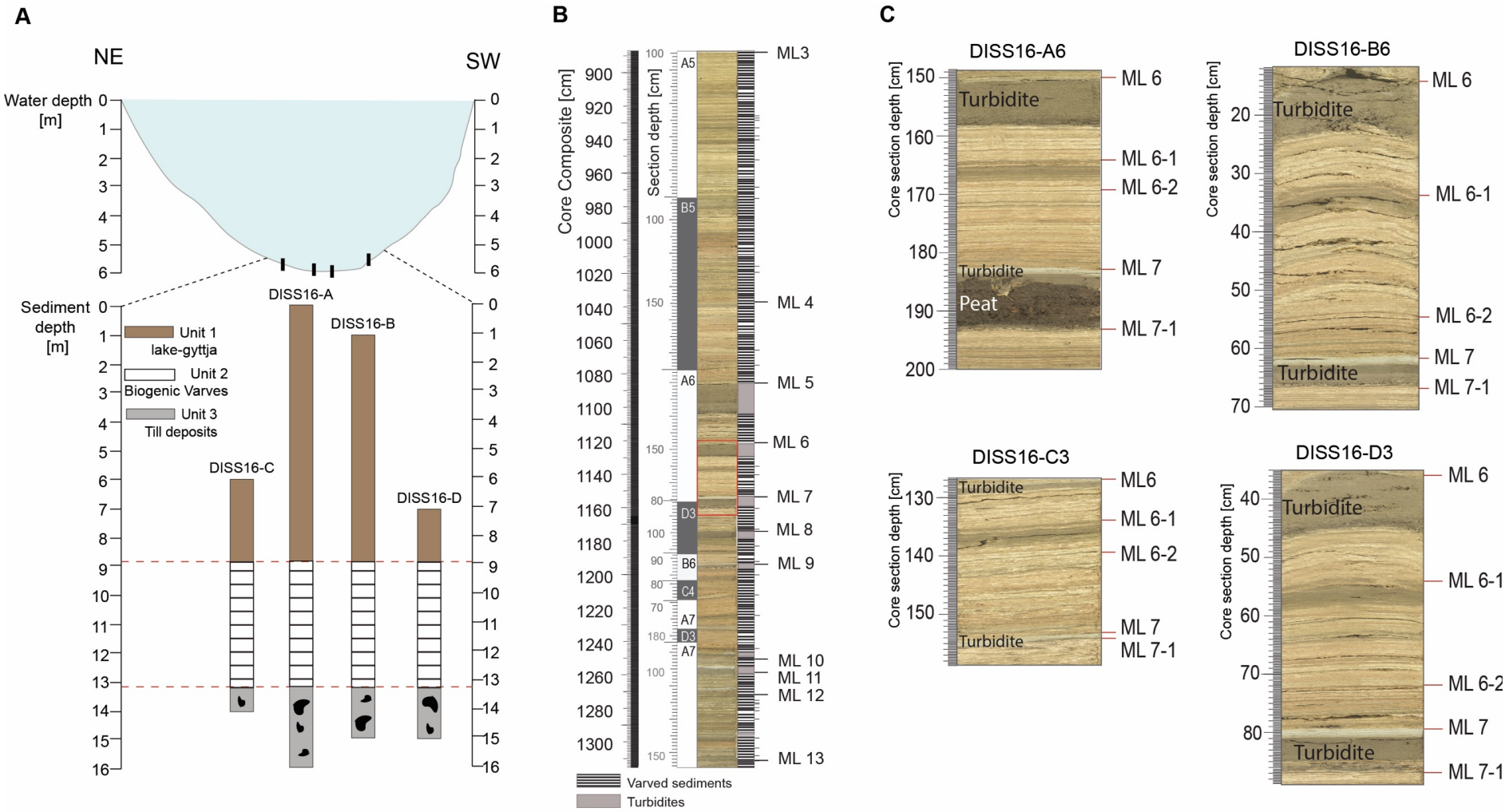

Figure 2. Diss Mere stratigraphy. (**A**) Stratigraphic correlation of the Diss Mere cores and sedimentary units. Cores are shown in a NE-SW section through the lake. (**B**) Core photo and stratigraphy of the DISS-16 composite profile showing the varved sequence of the record. Marker layers used for core correlation are shown. (**C**) Core photos of a min-section (11.22 – 11.6 m) of the sediment record in the four different cores. Macroscopically visible marker layers (ML6 to ML 7-1) used for core correlation are shown.

DISS16-A but it is only 10-cm thick (between marker layer ML 7 and ML 7-1, Fig. 2c) and is not present in the other cores. Fortunately, the combination of our four parallel cores into a composite profile has allowed the identification of a continuous laminated sequence of 4.2 m in length (unit 2, Fig. 2b). The transition between unit 3 and 2 is sharp, however there are slumps that show distorted laminated sediments at the top of unit 3 that might indicate lamination preservation earlier in the lake's history. The transition between unit 2 and unit 1 is diffuse and the lamination fades out over the last four laminae. This could suggest a change in the lake system from meromictic to monomictic (present) conditions caused by the infilling and therefore shallowing of the lake (Boehrer and Schultze, 2008).

Microfacies analyses of the laminated sediments confirm the presence of varves (pale-dark couplets) along the whole Unit 2 (Fig. 3) that are comparable to the model proposed by Peglar et al. (1984). We have also identified three different varve microfacies that reflect interannual variability in the varve composition (Fig. 3a). Microfacies 1 consists of a pale layer made of authigenic calcite crystals and diatom frustules, and a dark layer composed of, primarily, planktonic centric diatoms and filaments of organic matter (Microfacies 1a). Occasionally, an additional layer made of unstructured organic matter only occurs following the dark layer (Microfacies 1b). Microfacies 2 is similar to microfacies 1 but includes a mono-specific diatom bloom layer preceding the calcite layer. Microfacies 3 are varves with an occasional very thin calcite layer and mono-specific diatom blooms in spring and autumn. While the composition of diatom species varies across the varved section, the two blooms can be distinguished because the size of the diatoms in the spring blooms are smaller than the diatoms in the autumn bloom. The size of the authigenic calcite crystals in microfacies 1 and microfacies 2 also shows interannual variability. The two types of calcite layers are described as follows: a calcite lamina composed of micritic calcite crystals (< 4 μm; Bailey, 2005) (Fig. 3b) and a calcite layer with coarser crystal at the bottom with the size of the crystals decreasing upward through the lamina (62 – 5 μm; Bailey, 2005) (Fig. 3b). The occurrence of one type of calcite layer or another is quite random along the whole record and we have not found a clear relationship to specific microfacies.

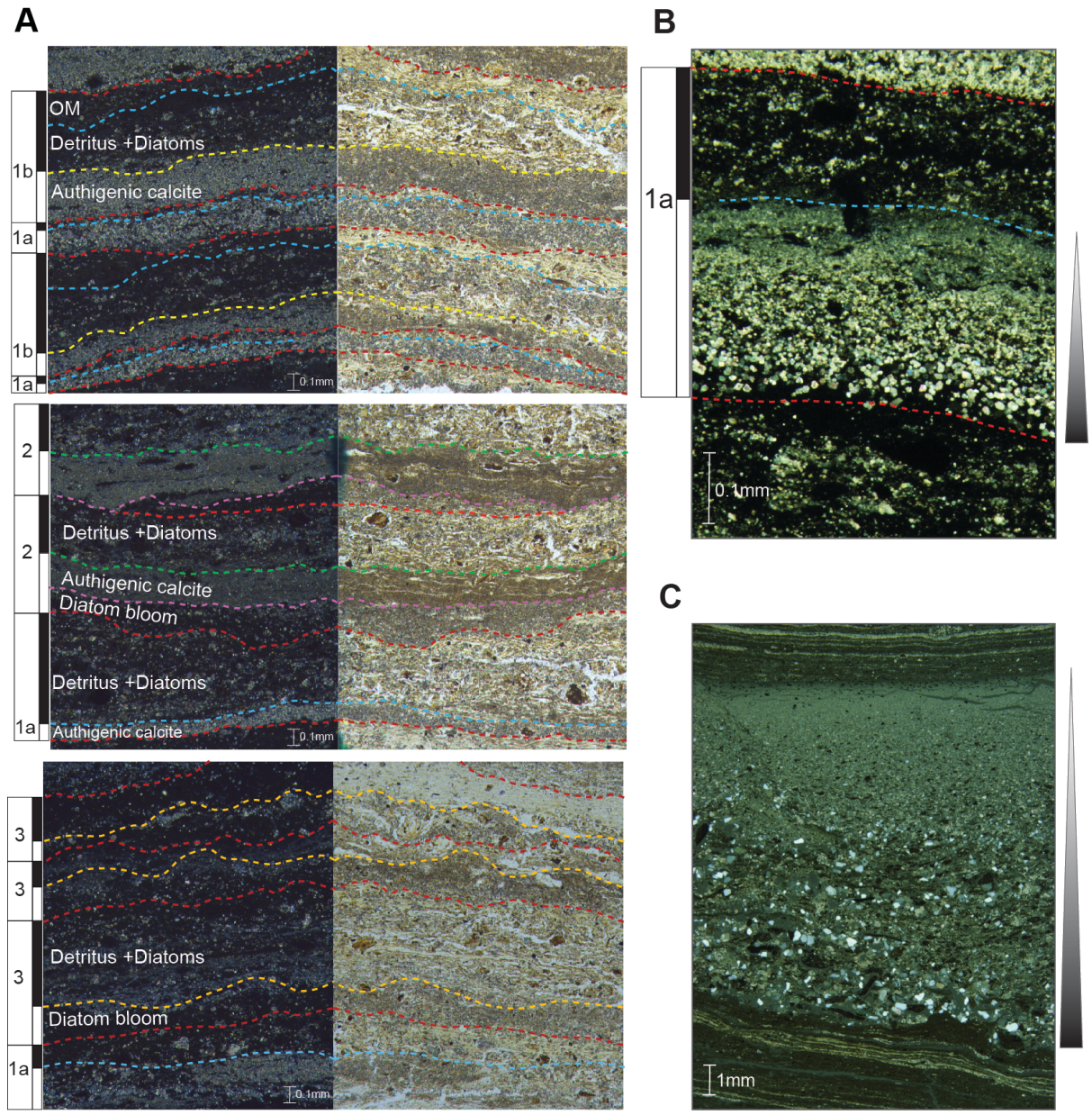

Figure 3. A. Microscope images of the varved sediments showing the pale (calcite) - dark (diatoms and organic matter) couplet, normal light (left) and polarised light (right). (**B**) Microscope image of a varve showing the gradual decrease of the calcite grains within the pale layer. (**C**) Microscope image of a lake turbidite deposited in the varved sediments (ML 12-7).

296

297 The varve sequence is occasionally interrupted by a total of 31 massive deposits (0.5 mm -
298 200 mm thick) between 10.35 and 13.15 m. These deposits are graded layers composed of
299 quartz grains in a matrix of calcite mud with sharp contacts to the succeeding varve (Fig. 3c).
300 These sediments are interpreted as lake turbidites, either from high discharge events or
301 sediment instability at the sub-aerial margins. Inter-core comparison of these deposits

suggests that the thickness of the lake turbidites is variable over short distances (e.g Fig. 2c), but varve thickness measurements are consistent between cores.

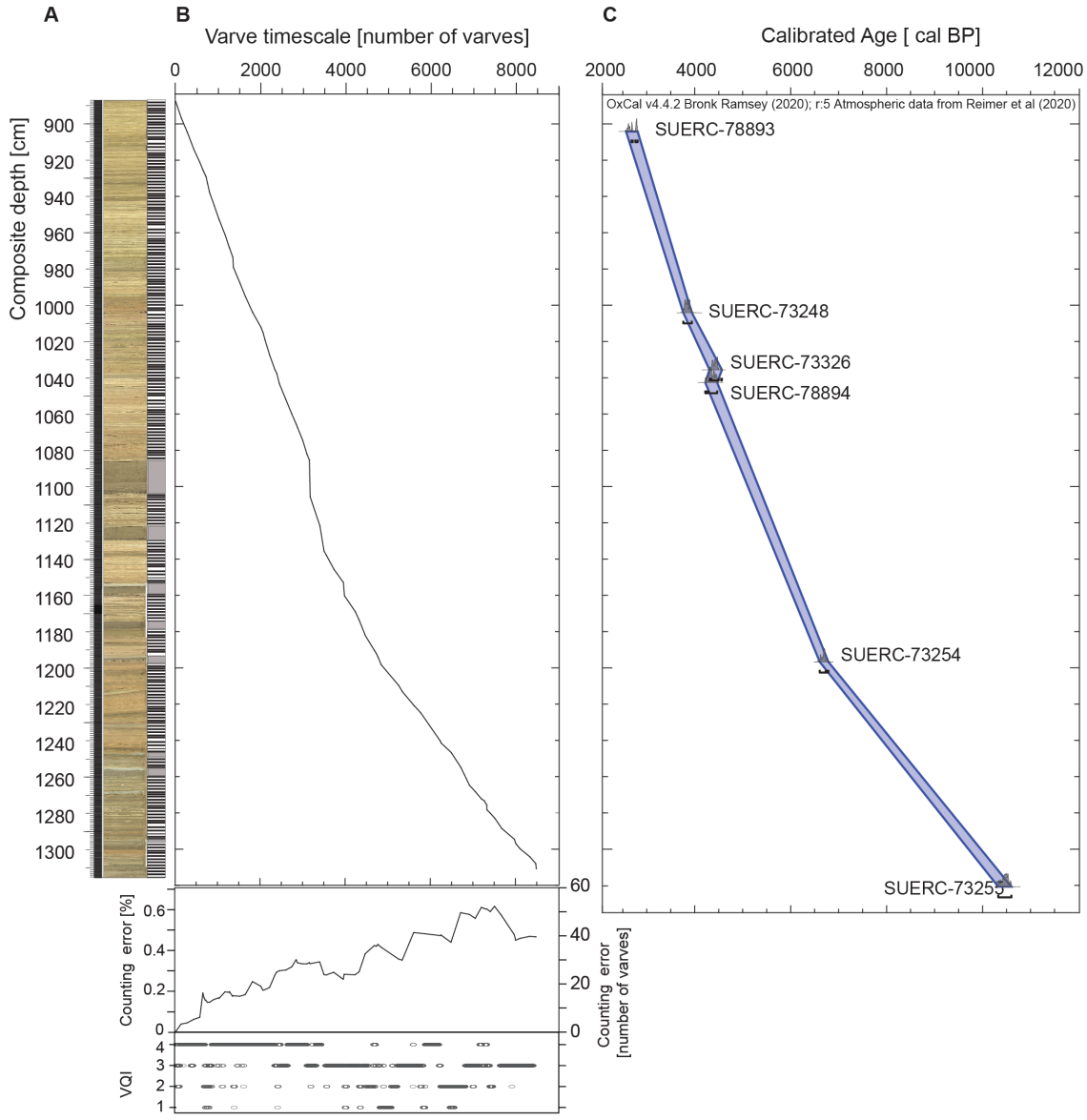

Figure 4. Diss Mere varve chronology. (**A**) DISS-16 composite profile. (**B**) Varve chronology: the black line is the master varve count record with the associated counting error in orange; below, the cumulative counting error (2σ standard deviation) is shown as both percentage and number of varves; Varve Quality Index (VQI) ranging the varve preservation from 4 (very well preservation) to 1 (poor preservation). (**C**) Radiocarbon age-depth model for Diss Mere; depth model output for the dates listed in Table 1 (P_Sequence, where z is defined as sediment depth; OxCal v4.4.2, Bronk Ramsey, 2008; r:5 Atmospheric data from Reimer et al. 2020). In grey, the likelihood distribution for the single calibrated dates. In blue, the 95.4% highest probability density range plotted as an age-depth model.

Table 1. Radiocarbon dates. List of the terrestrial macrofossils dated with the AMS radiocarbon method. The calibrated dates were calculated according to the IntCal20 curve (Reimer et al., 2020).

Lab code	Material	$\delta^{13}C$ relative to VPDB (‰)	Composite Depth (cm)	Radiocarbon Age BP	Calibrated date BP
SUERC-78893 (GU47750)	Bud and Wood	-28.3	904.6	2538 ± 24	2621 ± 121
SUERC-73248 (GU43847)*	Fruit	-24.1	1004.5	3519 ± 29	3788 ± 89
SUERC-73326 (GU43848R)*	Acorn	-24.4	1036	3927 ± 29	4376 ± 129
SUERC-78894 (GU47751)*	Wood	-27	1043	3863 ± 24	4282 ± 124
SUERC-73254 (GU43850)*	Fruit	-25.2	1197	5826 ± 24	6644 ± 90
SUERC-73255 (GU43852)*	Seeds, leaves	-25	1321	9262 ± 34	10429 ± 137

*Selected dates for Bayesian age modelling

5.2. Varve chronology

A total of 8473 varves have been counted downcore along 427 cm in the composite profile DISS-16, 888 – 1315 cm (Fig. 4a, b). The average VQI is 3.13, which indicates that the varves are well-preserved along the study interval (Fig. 4b). In sections where VQI is 1 (Fig. 4b), 976 of the 8473 varves were counted but varve thickness was not measured. Microfacies observations show that these intervals correspond to laminated sediments (microfacies 3) with an average varve thickness of 0.125 mm. The thin varves and the absence of the pale lamina precluded a precise varve counting within these intervals. Despite this varve interpolation, the varve chronology has varve counting errors below 0.62 % (Fig. 4b). The sedimentation rates within the study interval are rather uniform with an average varve thickness of 0.425 mm. There are, however, a few abrupt but not significant changes in the sedimentation rate, which are linked to the deposition of thick lake turbidite layers up to a cm scale (Fig. 2b, c, 3c).

The AMS^{14}C dates were initially compared to the varve chronology. Radiocarbon dating of the Diss Mere sediments places the varved sequence between ca 2500 and 10,500 cal BP, covering much of the Holocene period (Fig. 4c).

5.3. Tephrochronology

The results of cryptotephra investigations throughout the varved record of Diss Mere show two discrete tephra layers at the top of the sequence corresponding to known volcanic

eruptions in the Late Holocene (Fig. 4d), which can be used as stratigraphic isochrones to validate the varve chronology.

DISS16_T888.5, Glen Garry tephra (888.3 – 888.8 cm)

A peak of this tephra layer was found in a 0.5 cm interval at the composite depth of 888.5 cm. This layer is predominantly comprised of colourless, cuspate, fluted and open vesicular glass shards (4,035 shards g^{-1}. A few intermediate, blocky glass shards were encountered (63 shards g^{-1}) (Fig. 4d). Thirteen geochemical analyses classify this tephra layer as a sub-alkali rhyolite. The geochemical characteristics of this layer suggest a correlation to the Glen Garry (GGT) with diagnostic potassium, calcium, magnesium and iron contents which distinguish it from other silicic tephras of this provisional time interval (Dugmore et al., 1995) (Fig. 5, Table S.1). First detected in peat deposits in central Scotland (Dugmore et al., 1995), the GGT is widely reported from sites in northern Britain (Pilcher and Hall, 1996; Barber et al., 2008) . In northern Germany, van den Bogaard and Schmincke (2002) attribute the DOM-5 tephra, which has been identified within a series of peat deposits to the GGT, and Wulf et al. (2016) report the tephra within the annually-laminated (varved) sediment section of Lake Tiefer See. An age of 2170 ± 110 cal BP for this tephra horizon has been derived from the varve-based chronology by Dräger et al. (2017). The volcanic source of the GGT is uncertain, however, (Gudmundsdóttir et al., 2016) have recently deemed it indistinguishable from a rhyolitic tephra associated with the A~2000 eruption of the Askja volcanoand identified in two sites around the Vatnajökull ice cap in Iceland (Óladóttir et al., 2011).

DISS16_T921.5, OMH-185 tephra (921.3-921.8 cm)

This discrete tephra layer was confined within 0.5 cm at a composite depth of 921.5 cm (Fig. 4d). The dense, colourless glass shards encountered at this layer were typically cuspate with large, open, rounded vesicles (1,742 shards g^{-1}) and a defining feature of many is the presence of microlitic inclusions. Small quantities of intermediate, blocky glass shards were also identified (33 shards g^{-1}) (Fig. 4d). According to fifteen geochemical analyses shown in Figure 6 and Table S.1, the layer can be classified as a sub-alkali rhyolite and is correlated with the OMH-185 (‘Barnsmore’) tephra layer (Hall and Pilcher, 2002). The OMH-185 has been

identified in peat profiles within Ireland where it has been dated to 755–680 cal BC (2705–2630 cal. BP) (Plunkett et al., 2004) and in south-west Britain at Roman Lode, Devon (Matthews, 2008). In Scotland, the tephra layer has been recognised as the BGMT-3 (Langdon and Barber, 2001) whilst in Germany it has been termed the DOM-6 microlite (van den Bogaard and Schmincke, 2002). Plunkett and Pilcher (2018) highlight a reported compositional match to a rhyolitic tephra termed the SAU-65, which is thought to have been produced by an unidentified source beneath the Vatnajökull ice cap in Iceland (Larsen and Eiríksson, 2008).

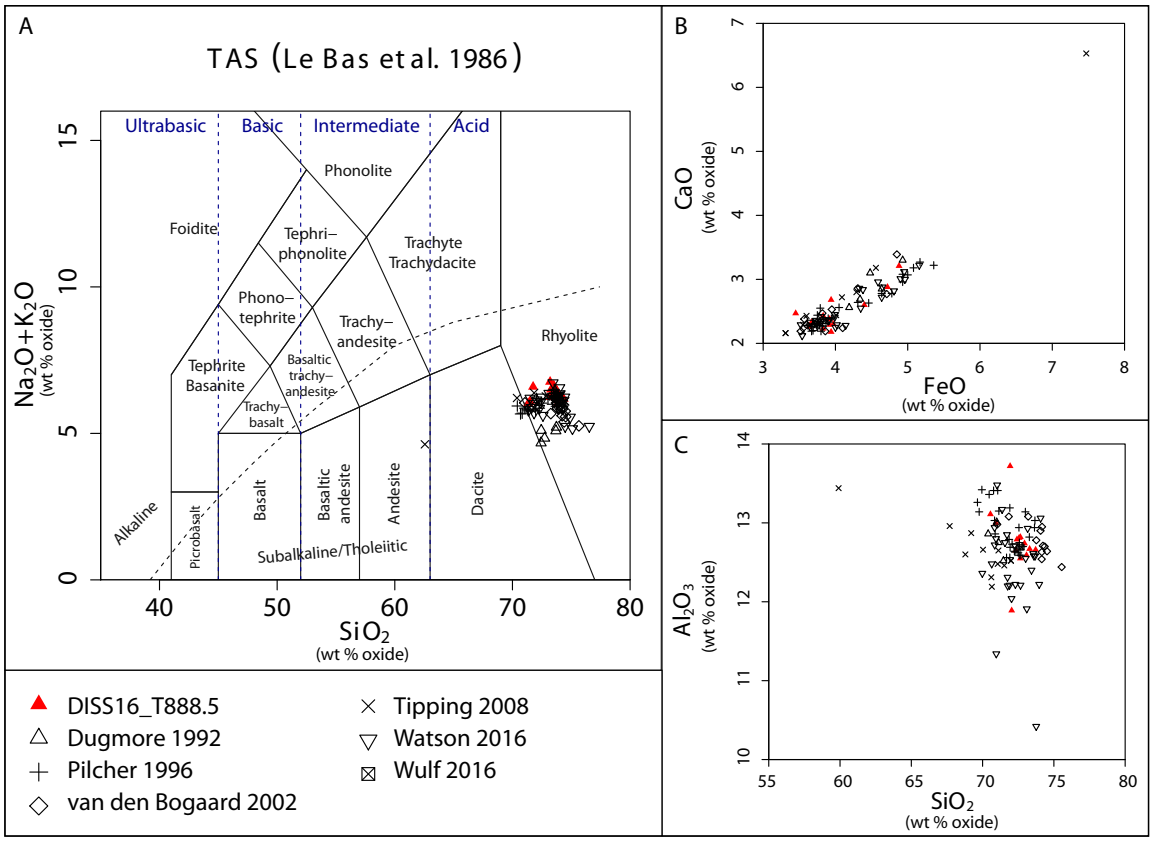

Figure 5. Figure 5. Chemical bi-plots of EPMA-derived major element chemical data from DISS16_T888.5 data are plotted as non-normalised wt% oxides with a cut off of 95% analytical total, see supplementary information for all data. These are compared against reference data from the RESET database (http://c14.arch.ox.ac.uk/reset/) and Tephrabase (www.tephrabase.org) (Newton et al., 2007). (A) Total alkali versus silica (TAS) classification (Le Bas et al., 1986). (B) FeO vs CaO. (C) SiO_2 vs Al_2O_3.

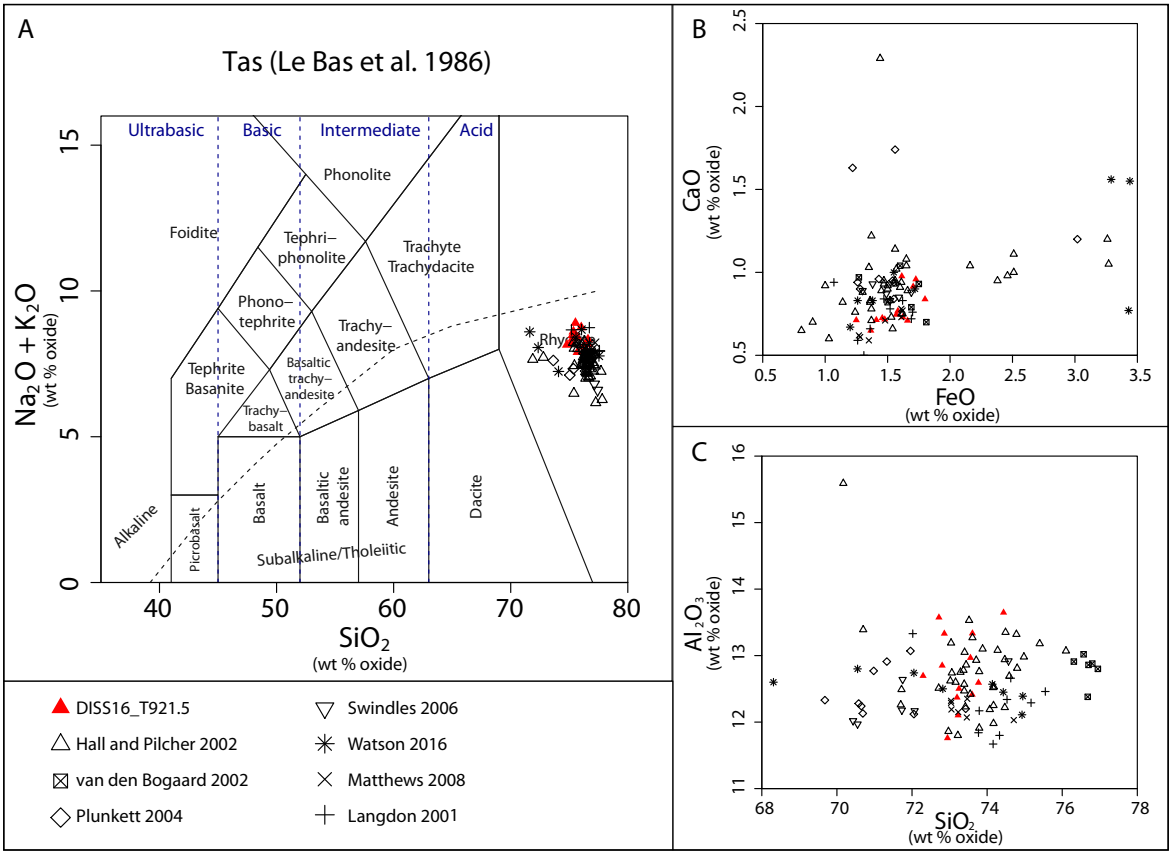

Figure 6. Chemical bi-plots of EPMA-derived major element chemical data from DISS16_T921.5 data are plotted as non-normalised wt% oxides with a cut off of 95% analytical total, see supplementary information for all data. These are compared against reference data from the RESET database (http://c14.arch.ox.ac.uk/reset/) and Tephrabase (www.tephrabase.org) (Newton et al., 2007). (A) Total alkali versus silica (TAS) classification (Le Bas et al.,1986). (B) FeO vs CaO. (C) SiO_2 vs Al_2O_3.

5.5. Bayesian age modelling: integration of different dating methods

The six radiocarbon dates from the varve section of Diss Mere were combined with dating information from the two identified tephra layers. For the Glen Garry tephra radiocarbon ages associated with this tephra are reported in Barber et al. (2008), with a Bayesian wiggle match age from the BPEAT software of 2174 cal BP (with a range of 224 years, 2210-1966 cal BP at 95%), using the IntCal04 calibration curve (Reimer et al., 2004). Recently, as mentioned earlier, the age for the Glen Garry has been refined by its identification in varved Tiefer See in northern Germany to 2170 ± 110 cal BP (Dräger et al., 2017). For the OMH-185 tephra the age was again based on a wiggle match estimate, in this case through a sequence of radiocarbon dates from Irish peat deposits as Glen West, county Fermanagh (Plunket et al., 2004). At Glen West the OMH-185 was part of a suite of tephra constrained by five radiocarbon dates. The radiocarbon ages were wiggle matched to the IntCal98 calibration curve using a

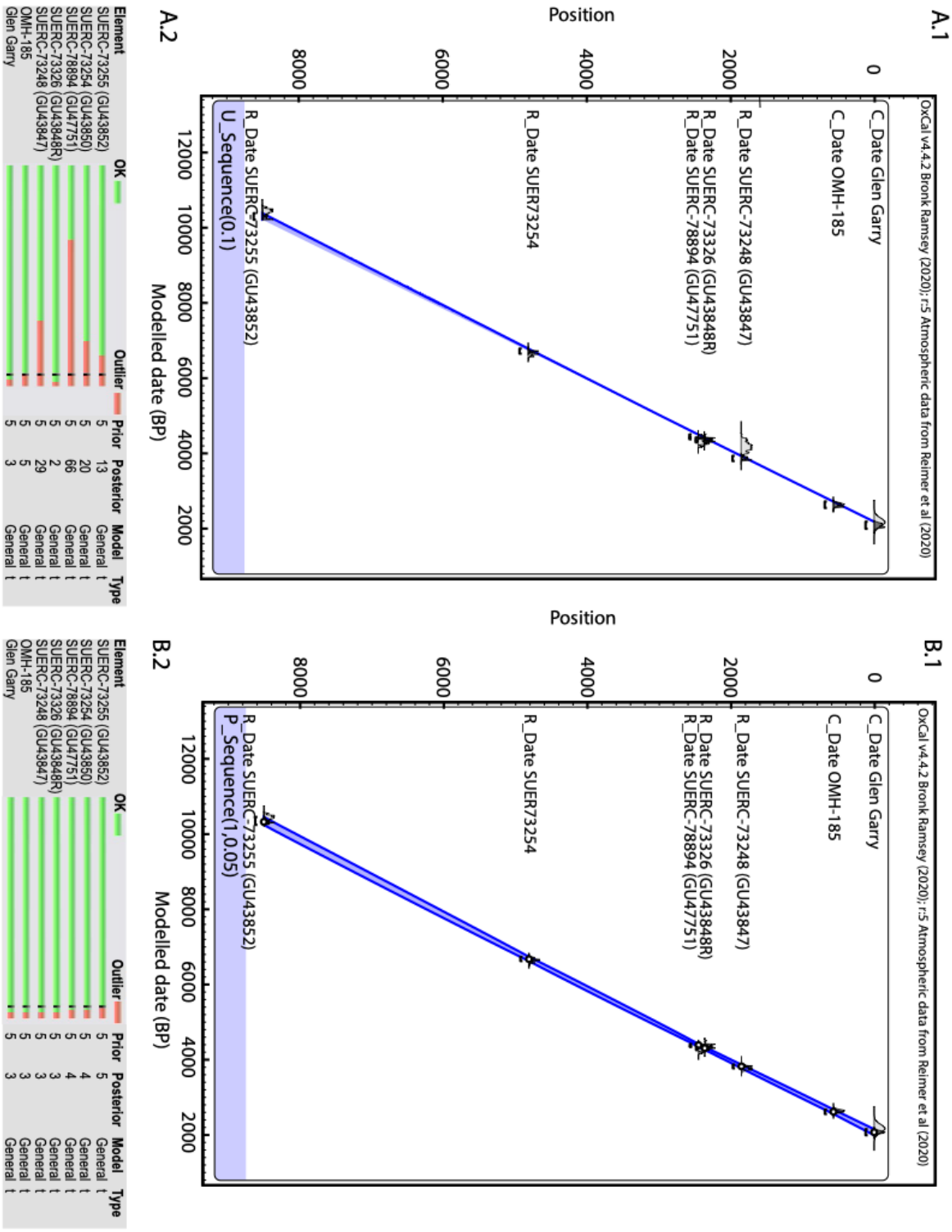

Figure 7. Bayesian age-depth models for Diss Mere: A.1 is a *U_Sequence* deposition model and A.2 shows outlier model results; B.1 is a *P_Sequence* deposition model and B2. shows outlier model results using OxCal 4.3 (Bronk-Ramsey, 2008). For details of the model construction see text.

382 variable or *V-Sequence* age model, with the age spacing between dates being based on a
383 liner regression through the mid-point of the calibrated age ranges. In order to develop an
384 IntCal20 age for the OMH-185 tephra the original radiocarbon dates have been recalibrated,
385 yielding an updated age for this tephra of 2651 ± 27 cal. BP (Supplementary information).
386 In order to combine the radiocarbon dates and the calendar ages for the tephra two slightly
387 different age modelling experiments were attempted, based on approaches derived from
388 Bayesian deposition modelling of other varved sequences (Bronk Ramsey, 2008; Blockley et
389 al., 2008; Lane et al., 2011). The aim was to find a deposition modelling approach that was
390 sufficiently constrained to reflect the fact that Diss Mere is annually resolved, but at the same
391 time to allow for the uncertainty in anchoring the floating varve chronology to the IntCal20
392 (Reimer et al., 2020) calibration curve. This includes the depositional processes within lakes
393 that mean that there is the potential for missing varves or occasionally disturbed varves that
394 require interpolation. The two Bayesian deposition models for Diss Mere are shown in Figure
395 7 and the full model is available as supplementary information. The topmost radiocarbon date
396 SUERC 78893 was rejected by both models because it is 99% outlying from the deposition
397 models. This date (2621 ± 121 cal BP) is located 17 cm above the tephra layer OMH-185
398 (2651 ± 27 cal. BP). The two time-markers are separated by 312 varve years, which suggests
399 this radiocarbon date might provide older ages than expected. We have, thus, excluded this
400 from the final age-depth model.
401 The *U_Sequence* model (Fig. 7a) with maximum rigidity assumes a linear rate of varve
402 formation between fixed points. This model is very precise, with errors at 95% confidence
403 between 11 and 37 years. However, the model suggests that SUERC 73248 (18%) and 78894
404 (6%) are both partial outliers and has down-weighted both proportionally. As there is no prior
405 reason to assume these dates are suspect it is likely that the model assumptions are slightly
406 too constrained to fully reflect the periods of uncertain varve preservation (VQI ≤ 2).
407 The *P_Sequence* model (Fig. 7b) with a fixed K value (0.5) is plotted alongside the outlier
408 evaluation. This model is almost as precise as the *U_Sequence* with errors at 95.4%
409 confidence of 16 to 55 years. Crucially this level of chronological precision allows decadal to

centennial scale events to be resolved but all of the dates fully contribute to the model and no outliers are detected, except for the radiocarbon date SUERC 78893 mentioned above. The *P_Sequence* model is thus accepted as the best approach for anchoring the floating varve chronology to the calendar - year timescale. The model begins at varve year 8 (the position of the Glen Garry tephra) and runs until the position of the lowest radiocarbon date at 132.1 cm of sediment depth (Fig. 7b). This gives a basal age for the onset of varve formation (131.5 cm of sediment depth) in Diss Mere of 10,290 ± 55 cal BP. There is, however, a difference of 252 years between the floating varve chronology (8473 ± 41 varves) and the *P_Sequence* model (8221 ± 55 modelled years) that could be explained by overcounted varves. As mentioned above 976 varves (type 3) were estimated in sections where the VQI is 1. The comparison of the two timescales suggests that 252 of these 976 varves may have been overcounted, and demonstrates that the *P_Sequence* model is the most robust chronology for the Diss Mere record.

6. Final considerations and Conclusions

The final chronology for the varved sediments of Diss Mere (DISSV-2020) integrates Bayesian age modelling and varve counting for the time period between 2069 ± 39 and 10,290 ± 55 cal BP. DISSV-2020 represents the most precise Holocene age model available from annually-resolved lake sediments in the British Isles, and is matched by only a very few records around the world.

Given this robust chronology, we presume that further research into the Diss Mere record may have significant implications in the following research areas:

- Palaeoclimatology. The potential for the Diss Mere record as a high-resolution palaeoclimate archive for the British Isles, in particular, and the North Atlantic region, in general, is enhanced by the location of the Glen Garry (2073 ± 39 cal BP) and the OMH-185, (2617 ± 29 cal BP), which allows cross correlation between records from different geographical locations in Europe during the period around 2.0 – 3.0 cal. ka BP. This is highly significant as this period contains the Homeric climate oscillation (ca.

2.75 ka BP), one of the most significant abrupt climate change of the Late Holocene, coinciding with the Homeric grand solar minimum and the radiocarbon calibration Hallstatt plateau (ca. 750 – 400 cal BC) (van Geel et al., 1999), and only a few independently-dated climate records provide evidence to test forcing mechanisms behind this climate change (Martin-Puertas et al., 2012). Moreover, within the period of varved sediments in Diss Mere, there are also Mid- and Early Holocene short-lived climatic fluctuations that have been recognised in lake, peat, ice-core and speleothem records, such as the 4.2, the 8.2, the 9.3 and the 10.3 ka BP climatic fluctuations, with different proposed drivers (e.g. Blockley et al., 2018), and the possibility that some of these events may be blurred by the chronological uncertainty inherent in many records. The DISSV-2020 chronology offers the possibility to examine the expression of these events at very high resolution within Britain, and to explore seasonal changes, as well as shifting environmental responses across the abrupt oscillations.

- Tephrochronology. The potential for additional tephra layers deposited within the varves will contribute to the development of a Holocene European-wide tephrostratigraphic and tephrochronological framework. For example, the annual resolution of the sediments may allow multiple eruptions from the same or different sources and that occur over short time intervals to be distinguished. In turn this will generate improved precision on the time intervals between eruptions, an approach currently limited to rare examples in the Late Glacial (Lane et al., 2013).
- Archaeology. The Diss Mere varved sequence has the potential to refine the picture of the interaction between humans and their environment in East Anglia from the Mesolithic onwards. Sub-decadal scale palaeolimnological and palaeoecological studies are key to evaluate and understand the late development of farming and sedentism in Norfolk, the duration of the Bronze Age in this region and human impacts on the landscape into the Late Iron Age (Medlycott, 2011).

Acknowledgements

This study is funded by the Royal Society (ref: DH150185) and the Natural Environment Research Council (NE/L002485/1). This paper is a contribution to the Varved Sediments Database (VARDA) and data are available at https://varve.gfz-potsdam.de/. The authors thank the technical coring team Brian Brademann and Markus Schwab for recovering excellent cores, and Dr. Chris Hayward at the Tephra Analysis Unit (TAU), University of Edinburgh for his support and assistance with the geochemical analyses. Special thanks to Professor Jim Rose for valuable comments on the geology of the site, Professor John Lowe for expert advice through research on Diss Mere, and Dr. Ian Bailey for comments and suggestions on a previous version of the manuscript. The authors also thank the editor Prof. Siwan Davies as well as Prof. Bernd Zolitschka and an anonymous reviewer for their comments and suggestions, which improved the submitted manuscript. The authors are grateful to the Diss Council for providing accessibility to the lake and local support during the coring campaign.

References

Bailey, I., 2005. A high-resolution record of mid-Holocene climate change from Diss Mere, UK. (Doctoral). Dr. Thesis Univ. Lond. University of London.

Barber, K., Langdon, P., Blundell, A., 2008. Dating the Glen Garry tephra: a widespread late-Holocene marker horizon in the peatlands of northern Britain: The Holocene. https://doi.org/10.1177/0959683607085594

Bennett, K.D., 1983. Devensian Late-Glacial and Flandrian Vegetational History at Hockham Mere, Norfolk, England. New Phytol. 95, 457–487. https://doi.org/10.1111/j.1469-8137.1983.tb03512.x

Blockley, S.P.E., Bronk Ramsey, C., Pyle, D.M., 2008. Improved age modelling and high-precision age estimates of late Quaternary tephras, for accurate palaeoclimate reconstruction. J. Volcanol. Geotherm. Res., Explosive volcanism in the central Mediterranean area during the late Quaternary - linking sources and distal archives 177, 251–262. https://doi.org/10.1016/j.jvolgeores.2007.10.015

Blockley, S.P.E., Lane, C.S., Lotter, A.F., Pollard, A.M., 2007. Evidence for the presence of the Vedde Ash in Central Europe. Quat. Sci. Rev. 26, 3030–3036. https://doi.org/10.1016/j.quascirev.2007.09.010

Blockley, S.P.E., Pyne-O'Donnell, S.D.F., Lowe, J.J., Matthews, I.P., Stone, A., Pollard, A.M., Turney, C.S.M., Molyneux, E.G., 2005. A new and less destructive laboratory procedure for the physical separation of distal glass tephra shards from sediments. Quat. Sci. Rev. 24, 1952–1960. https://doi.org/10.1016/j.quascirev.2004.12.008

Boehrer, B., Schultze, M., 2008. Stratification of lakes. Rev. Geophys. 46. https://doi.org/10.1029/2006RG000210

Brauer, A., Casanova, J., 2001. Chronology and depositional processes of the laminated sediment record from Lac d'Annecy, French Alps. J. Paleolimnol. 25, 163–177. https://doi.org/10.1023/A:1008136029735

Brauer, A., Endres, C., Zolitschka, B., Negendank, J.W., 2000. AMS radiocarbon and varve chronology from the annually laminated sediment record of Lake Meerfelder Maar, Germany. Radiocarbon 42, 355–368.

Brauer, A., Haug, G.H., Dulski, P., Sigman, D.M., Negendank, J.F.W., 2008. An abrupt wind shift in western Europe at the onset of the Younger Dryas cold period. Nat. Geosci. 1, 520–523. https://doi.org/10.1038/ngeo263

Bronk Ramsey, C., 2009. Bayesian Analysis of Radiocarbon Dates. Radiocarbon 51, 337–360. https://doi.org/10.1017/S0033822200033865

Bronk Ramsey, C., 2008. Deposition models for chronological records. Quat. Sci. Rev., INTegration of Ice-core, Marine and Terrestrial records (INTIMATE): Refining the record of the Last Glacial-Interglacial Transition 27, 42–60. https://doi.org/10.1016/j.quascirev.2007.01.019

Davies, S.M., 2015. Cryptotephras: the revolution in correlation and precision dating. J. Quat. Sci. 30, 114–130. https://doi.org/10.1002/jqs.2766

Dräger, N., Theuerkauf, M., Szeroczyńska, K., Wulf, S., Tjallingii, R., Plessen, B., Kienel, U., Brauer, A., 2017. Varve microfacies and varve preservation record of climate change and human impact for the last 6000 years at Lake Tiefer See (NE Germany). The Holocene 27, 450–464. https://doi.org/10.1177/0959683616660173

Dugmore, A.J., Larsen, G., Newton, A.J., 1995. Seven tephra isochrones in Scotland. The Holocene 5, 257–266. https://doi.org/10.1177/095968369500500301

Farr, K.M., Jones, D.M., O'Sullivan, P.E., Eglinton, G., Tarling, D.H., Hedges, R.E.M., 1991. Palaeolimnological studies of laminated sediments from the Shropshire-Cheshire meres. Hydrobiologia 214, 279–292. https://doi.org/10.1007/BF00050962

Gudmundsdóttir, E.R., Larsen, G., Björck, S., Ingólfsson, Ó., Striberger, J., 2016. A new high-resolution Holocene tephra stratigraphy in eastern Iceland: Improving the Icelandic and North Atlantic tephrochronology. Quat. Sci. Rev. 150, 234–249. https://doi.org/10.1016/j.quascirev.2016.08.011

Hall, V.A., Pilcher, J.R., 2002. Late-Quaternary Icelandic tephras in Ireland and Great Britain: detection, characterization and usefulness. The Holocene 12, 223–230. https://doi.org/10.1191/0959683602hl538rr

Hayward, C., 2011. High spatial resolution electron probe microanalysis of tephras and melt inclusions without beam-induced chemical modification. The Holocene 22, 119–125. https://doi.org/10.1177/0959683611409777

Lane, C.S., Blockley, S.P.E., Ramsey, C.B., Lotter, A.F., 2011. Tephrochronology and absolute centennial scale synchronisation of European and Greenland records for the last glacial to interglacial transition: A case study of Soppensee and NGRIP. Quat. Int. 246, 145–156. https://doi.org/10.1016/j.quaint.2010.11.028

Lane, C. S., Brauer, A., Blockley, S.P.E., Dulski, P., 2013. Volcanic ash reveals time-transgressive abrupt climate change during the Younger Dryas. Geology 41, 1251–1254. https://doi.org/10.1130/G34867.1

Lane, Christine S., Brauer, A., Blockley, S.P.E., Dulski, P., 2013. Volcanic ash reveals time-transgressive abrupt climate change during the Younger Dryas. Geology 41, 1251–1254. https://doi.org/10.1130/G34867.1

Lane, C.S., Brauer, A., Martín-Puertas, C., Blockley, S.P.E., Smith, V.C., Tomlinson, E.L., 2015. The Late Quaternary tephrostratigraphy of annually laminated sediments from Meerfelder Maar, Germany. Quat. Sci. Rev. 122, 192–206. https://doi.org/10.1016/j.quascirev.2015.05.025

Langdon, P.G., Barber, K.E., 2001. New Holocene tephras and a proxy climate record from a blanket mire in northern Skye, Scotland. J. Quat. Sci. 16, 753–759. https://doi.org/10.1002/jqs.655

Larsen, G., Eiríksson, J., 2008. Late Quaternary terrestrial tephrochronology of Iceland—frequency of explosive eruptions, type and volume of tephra deposits. J. Quat. Sci. 23, 109–120. https://doi.org/10.1002/jqs.1129

559 Le Bas, M.J., Maitre, R.W.L., Streckeisen, A., Zanettin, B., 1986. A Chemical Classification
560 of Volcanic Rocks Based on the Total Alkali-Silica Diagram. J. Petrol. 27, 745–750.
561 https://doi.org/10.1093/petrology/27.3.745
562 Lee, J.R., Haslam, R., Woods, M.A., Rose, J., Graham, R.L., Ford, J.R., Schofield, D.I.,
563 Kearsey, T.I., Williams, C.N., 2020. Plio-Pleistocene fault reactivation within the Crag
564 Basin, eastern UK: implications for structural controls of landscape development
565 within an intraplate setting. Boreas n/a. https://doi.org/10.1111/bor.12462
566 Lowe, D.J., 2011. Tephrochronology and its application: A review. Quat. Geochronol. 6,
567 107–153. https://doi.org/10.1016/j.quageo.2010.08.003
568 Martin-Puertas, C., Lauterbach, S., Allen, J.R.M., Perez, M., Blockley, S., Wulf, S., Huntley,
569 B., Brauer, A., 2019. Initial Mediterranean response to major climate reorganization
570 during the last interglacial-glacial transition. Quat. Sci. Rev. 215, 232–241.
571 https://doi.org/10.1016/j.quascirev.2019.05.019
572 Martin-Puertas, C., Matthes, K., Brauer, A., Muscheler, R., Hansen, F., Petrick, C., Aldahan,
573 A., Possnert, G., van Geel, B., 2012a. Regional atmospheric circulation shifts
574 induced by a grand solar minimum. Nat. Geosci. 5, 397–401.
575 https://doi.org/10.1038/ngeo1460
576 Martin-Puertas, C., Matthes, K., Brauer, A., Muscheler, R., Hansen, F., Petrick, C., Aldahan,
577 A., Possnert, G., van Geel, B., 2012b. Regional atmospheric circulation shifts
578 induced by a grand solar minimum. Nat. Geosci. 5, 397–401.
579 https://doi.org/10.1038/ngeo1460
580 Matthews, I., 2008. Roman Lode, Exmoor, Devon: Tephrochronology Scientific Dating
581 Report. Res. Dep. Rep Ser.
582 Medlycott, M., 2011. Research and Archaeology Revisited: a revised framework for the East
583 of England. East Anglian Archaeology.
584 Nakov, T., Guillory, W., Julius, M., Theriot, E., Alverson, A., 2015. Towards a phylogenetic
585 classification of species belonging to the diatom genus Cyclotella
586 (Bacillariophyceae): Transfer of species formerly placed in Puncticulata ,
587 Handmannia , Pliocaenicus and Cyclotella to the genus Lindavia. Phytotaxa 217,
588 249–264. https://doi.org/10.11646/phytotaxa.217.3.2
589 Newton, A.J., Dugmore, A.J., Gittings, B.M., 2007. Tephrabase: tephrochronology and the
590 development of a centralised European database. J. Quat. Sci. 22, 737–743.
591 https://doi.org/10.1002/jqs.1094
592 Ojala, A.E.K., Francus, P., Zolitschka, B., Besonen, M., Lamoureux, S.F., 2012.
593 Characteristics of sedimentary varve chronologies – A review. Quat. Sci. Rev. 43,
594 45–60. https://doi.org/10.1016/j.quascirev.2012.04.006
595 Óladóttir, B.A., Larsen, G., Sigmarsson, O., 2011. Holocene volcanic activity at Grímsvötn,
596 Bárdarbunga and Kverkfjöll subglacial centres beneath Vatnajökull, Iceland. Bull.
597 Volcanol. 73, 1187–1208. https://doi.org/10.1007/s00445-011-0461-4
598 O'Sullivan, P.E., 1983. Annually-laminated lake sediments and the study of Quaternary
599 environmental changes — a review. Quat. Sci. Rev. 1, 245–313.
600 https://doi.org/10.1016/0277-3791(83)90008-2
601 Palmer, A.P., Matthews, I.P., Lowe, J.J., MacLeod, A., Grant, R., 2020. A revised
602 chronology for the growth and demise of Loch Lomond Readvance ('Younger Dryas')
603 ice lobes in the Lochaber area, Scotland. Quat. Sci. Rev. 248, 106548.
604 https://doi.org/10.1016/j.quascirev.2020.106548
605 Peglar, S.M., 1993a. The mid-Holocene Ulmus decline at Diss Mere, Norfolk, UK: a year-by-
606 year pollen stratigraphy from annual laminations. The Holocene 3, 1–13.
607 https://doi.org/10.1177/095968369300300101
608 Peglar, S.M., 1993b. The development of the cultural landscape around Diss Mere, Norfolk,
609 UK, during the past 7000 years. Rev. Palaeobot. Palynol. 76, 1–47.
610 https://doi.org/10.1016/0034-6667(93)90079-A
611 Peglar, S.M., Fritz, S.C., Alapieti, T., Saarnisto, M., Birks, H.J.B., 1984. Composition and
612 formation of laminated sediments in Diss Mere, Norfolk, England. Boreas 13, 13–28.
613 https://doi.org/10.1111/j.1502-3885.1984.tb00054.x

614 Peglar, S.M., Fritz, S.C., Birks, H.J.B., 1989. Vegetation and Land-Use History at Diss,
615 Norfolk, U.K. J. Ecol. 77, 203. https://doi.org/10.2307/2260925
616 Pilcher, J.R., Hall, V.A., 1996. Tephrochronological studies in northern England: The
617 Holocene. https://doi.org/10.1177/095968369600600112
618 Plunkett, G., Pilcher, J.R., 2018. Defining the potential source region of volcanic ash in
619 northwest Europe during the Mid- to Late Holocene. Earth-Sci. Rev. 179, 20–37.
620 https://doi.org/10.1016/j.earscirev.2018.02.006
621 Plunkett, G.M., Pilcher, J.R., McCormac, F.G., Hall, V.A., 2004. New dates for first
622 millennium BC tephra isochrones in Ireland: The Holocene.
623 https://doi.org/10.1191/0959683604hl757rr
624 Rach, O., Brauer, A., Wilkes, H., Sachse, D., 2014. Delayed hydrological response to
625 Greenland cooling at the onset of the Younger Dryas in western Europe. Nat.
626 Geosci. 7, 109–112. https://doi.org/10.1038/ngeo2053
627 Ramisch, A., Brauser, A., Dorn, M., Blanchet, C., Brademann, B., Köppl, M., Mingram, J.,
628 Neugebauer, I., Nowaczyk, N., Ott, F., Pinkerneil, S., Plessen, B., Schwab, M.J.,
629 Tjallingii, R., Brauer, A., 2020. VARDA (VArved sediments DAtabase) –
630 providing and connectingproxy data from annually laminated lake sediments
631 (preprint). Geosciences – Palaeooceanography, Palaeoclimatology.
632 https://doi.org/10.5194/essd-2020-55
633 Ramsey, C.B., Lee, S., 2013. Recent and Planned Developments of the Program OxCal.
634 Radiocarbon 55, 720–730.
635 Reimer, P.J., Austin, W.E.N., Bard, E., Bayliss, A., Blackwell, P.G., Ramsey, C.B., Butzin,
636 M., Cheng, H., Edwards, R.L., Friedrich, M., Grootes, P.M., Guilderson, T.P., Hajdas,
637 I., Heaton, T.J., Hogg, A.G., Hughen, K.A., Kromer, B., Manning, S.W., Muscheler,
638 R., Palmer, J.G., Pearson, C., Plicht, J. van der, Reimer, R.W., Richards, D.A., Scott,
639 E.M., Southon, J.R., Turney, C.S.M., Wacker, L., Adolphi, F., Büntgen, U., Capano,
640 M., Fahrni, S.M., Fogtmann-Schulz, A., Friedrich, R., Köhler, P., Kudsk, S., Miyake,
641 F., Olsen, J., Reinig, F., Sakamoto, M., Sookdeo, A., Talamo, S., 2020. The IntCal20
642 Northern Hemisphere Radiocarbon Age Calibration Curve (0–55 cal kBP).
643 Radiocarbon 62, 725–757. https://doi.org/10.1017/RDC.2020.41
644 Reimer, P.J., Baillie, M.G.L., Bard, E., Bayliss, A., Beck, J.W., Bertrand, C.J.H., Blackwell,
645 P.G., Buck, C.E., Burr, G.S., Cutler, K.B., Damon, P.E., Edwards, R.L., Fairbanks,
646 R.G., Friedrich, M., Guilderson, T.P., Hogg, A.G., Hughen, K.A., Kromer, B.,
647 McCormac, G., Manning, S., Ramsey, C.B., Reimer, R.W., Remmele, S., Southon,
648 J.R., Stuiver, M., Talamo, S., Taylor, F.W., Plicht, J. van der, Weyhenmeyer, C.E.,
649 2004. IntCal04 terrestrial radiocarbon age calibration, 0-26 cal kyr BP. Radiocarbon
650 46, 1029–1058.
651 Rose, J., 1994. Major river systems of central and southern Britain during the Early and
652 Middle Pleistocene. Terra Nova 6, 435–443. https://doi.org/10.1111/j.1365-
653 3121.1994.tb00887.x
654 Simola, H.L.K., Coard, M.A., O'Sullivan, P.E., 1981. Annual laminations in the sediments of
655 Loe Pool, Cornwall. Nature 290, 238–241. https://doi.org/10.1038/290238a0
656 Steffensen, J.P., Andersen, K.K., Bigler, M., Clausen, H.B., Dahl-Jensen, D., Fischer, H.,
657 Goto-Azuma, K., Hansson, M., Johnsen, S.J., Jouzel, J., Masson-Delmotte, V.,
658 Popp, T., Rasmussen, S.O., Röthlisberger, R., Ruth, U., Stauffer, B., Siggaard-
659 Andersen, M.-L., Sveinbjörnsdóttir, Á.E., Svensson, A., White, J.W.C., 2008. High-
660 Resolution Greenland Ice Core Data Show Abrupt Climate Change Happens in Few
661 Years. Science 321, 680–684. https://doi.org/10.1126/science.1157707
662 Sturm, M., Lotter, A.F., 1995. Lake sediments as environmental archives. EAWAG News 38
663 E, 6–9.
664 Timms, R.G.O., Matthews, I.P., Palmer, A.P., Candy, I., Abel, L., 2017. A high-resolution
665 tephrostratigraphy from Quoyloo Meadow, Orkney, Scotland: Implications for the
666 tephrostratigraphy of NW Europe during the Last Glacial-Interglacial Transition. Quat.
667 Geochronol., Advancing tephrochronology as a global dating tool: applications in

volcanology, archaeology, and palaeoclimatic research 40, 67–81. https://doi.org/10.1016/j.quageo.2016.06.004

Tippett, R., 1964. An investigation into the nature of the layering of deep-water sediments in two eastern ontario lakes. Can. J. Bot. 42, 1693–1709. https://doi.org/10.1139/b64-168

van der Bogaard, C. van den, Schmincke, H.-U., 2002. Linking the North Atlantic to central Europe: a high-resolution Holocene tephrochronological record from northern Germany. J. Quat. Sci. 17, 3–20. https://doi.org/10.1002/jqs.636

van Geel, B., Raspopov, O.M., Renssen, H., van der Plicht, J., Dergachev, V.A., Meijer, H.A.J., 1999. The role of solar forcing upon climate change. Quat. Sci. Rev. 18, 331–338. https://doi.org/10.1016/S0277-3791(98)00088-2

West, R.G., 1991. On the origin of Grunty Fen and other landforms in southern Fenland, Cambridgeshire. Geol. Mag. 128, 257–262. https://doi.org/10.1017/S001675680002210X

Wulf, S., Dräger, N., Ott, F., Serb, J., Appelt, O., Guðmundsdóttir, E., van den Bogaard, C., Słowiński, M., Błaszkiewicz, M., Brauer, A., 2016. Holocene tephrostratigraphy of varved sediment records from Lakes Tiefer See (NE Germany) and Czechowskie (N Poland). Quat. Sci. Rev. 132, 1–14. https://doi.org/10.1016/j.quascirev.2015.11.007

Wulf, S., Keller, J., Paterne, M., Mingram, J., Lauterbach, S., Opitz, S., Sottili, G., Giaccio, B., Albert, P.G., Satow, C., Tomlinson, E.L., Viccaro, M., Brauer, A., 2012. The 100–133 ka record of Italian explosive volcanism and revised tephrochronology of Lago Grande di Monticchio. Quat. Sci. Rev. 58, 104–123. https://doi.org/10.1016/j.quascirev.2012.10.020

Zolitschka, B., Brauer, A., Negendank, J.F.W., Stockhausen, H., Lang, A., 2000. Annually dated late Weichselian continental paleoclimate record from the Eifel, Germany. Geology 28, 783–786. https://doi.org/10.1130/0091-7613(2000)28<783:ADLWCP>2.0.CO;2

Zolitschka, B., Francus, P., Ojala, A.E.K., Schimmelmann, A., 2015. Varves in lake sediments – a review. Quat. Sci. Rev. 117, 1–41. https://doi.org/10.1016/j.quascirev.2015.03.019